Martian Crustal Field Influence on O+ and O2+ Escape as Measured by MAVEN

Tristan Weber, David Brain, Shaosui Xu, David Mitchell, Jared Espley,
Christian Mazelle, James P. Mcfadden, Bruce Jakosky

HAL Id: insu-03672408
https://insu.hal.science/insu-03672408

Martian Crustal Field Influence on O^+ and O_2^+ Escape as Measured by MAVEN

Tristan Weber[1], David Brain[1], Shaosui Xu[2], David Mitchell[2], Jared Espley[3], Christian Mazelle[4], James P. McFadden[2], and Bruce Jakosky[1]

[1]Laboratory for Atmospheric and Space Physics, University of Colorado, Boulder, CO, USA, [2]Space Science Laboratory, University of California, Berkeley, CA, USA, [3]Goddard Space Flight Center, Greenbelt, MD, USA, [4]IRAP, CNRS - University of Toulouse - UPS - CNES, Toulouse, France

Abstract Martian crustal magnetic fields influence the solar wind interaction with Mars in a way that is not fully understood. In some locations, crustal magnetic fields act as "mini-magnetospheres," shielding the planet's atmosphere, while in other locations they act as channels for enhanced energy input and particle escape. The net effect of this system is not intuitively clear, but previous modeling studies have suggested that crustal fields likely decrease global ion escape from Mars. In this study, we use data from the Mars Atmosphere and Volatile EvolutioN spacecraft to analyze how crustal magnetic fields influence both global and local ion escape at Mars. We find that crustal fields only increase ion escape if ions are not bound tightly to the magnetic field. Specifically, ion escape is increased only if closed magnetic fields trap 35% or less of energized oxygen ions. In any other case, crustal fields decrease both global and local ion escape by as much as 40% and 80%, respectively. This suggests that the presence of crustal magnetic fields has had a moderate impact on atmospheric ion loss throughout Martian history, potentially influencing the planet's atmospheric evolution and habitability.

Plain Language Summary The loss of the Martian atmosphere over time has transformed Mars from a potentially warm and wet planet to the cold, dry world we observe today. This atmospheric loss is often suggested to be the result of Mars losing its global magnetic field 3 billion years ago. However, the loss of a global dynamo did not leave the Martian system devoid of planetary magnetic fields. Rather, the crust of Mars still contains scattered pockets of magnetic field that extend outward into the planet's atmosphere. In some areas, these magnetic fields shield the planetary atmosphere much in the same way as the Earth's magnetic field, while in other areas the magnetic fields channel energy down into the planet's atmosphere, potentially driving enhanced atmospheric loss. In this study, we use spacecraft data from Mars Atmosphere and Volatile EvolutioN to analyze the extent to which Martian crustal magnetic fields affect atmospheric escape at Mars. We show that the shielding provided by crustal magnetic fields reduces present-day ion escape by as much as 40%, and suggest that over time this may have been an important factor in the total amount of atmosphere lost from the planet.

1. Introduction

Over the last three to four billion years, a majority of the initial Martian atmosphere has escaped to space, leading to drastic changes in the Martian climate that may have influenced the planet's habitability (Jakosky et al., 2018). Atmospheric escape occurs through a variety of physical mechanisms, and a primary goal of the Mars Atmosphere and Volatile EvolutioN (MAVEN) mission to Mars is to directly analyze the different escape processes present at Mars to determine their relative importance over time (Jakosky, Lin, et al., 2015).

In this study, we focus on the escape of planetary ions. Numerous spacecraft studies have found present-day global ion escape rates of $10^{24} - 10^{25}$ particles per second (Brain et al., 2015; Dong et al., 2015; Lundin et al., 1990, 2008; Nilsson et al., 2011; Ramstad et al., 2015; Vaisberg et al., 1977). If taken as a constant value through time, this would only account for the loss of a small fraction of the initial Martian atmosphere (a few mbar). However, from studies of other stars, it is expected that the sun was significantly more active early in the solar system (Ribas et al., 2005; Wood, 2006). With ~10 times the present-day EUV and X-ray intensity and ~10–100 times the present-day solar wind pressure, it is expected that ancient Mars would have experienced much higher rates of ionization and much stronger electric fields, leading to significantly

higher ion escape. We therefore find it necessary to study ion escape as it occurs at Mars today, such that we can understand how it may have varied throughout Martian history and contributed to the loss of the Martian atmosphere.

Because ions carry an electric charge, their motion is guided by the local magnetic environment, which at Mars is unique due to the presence of crustal magnetic fields. Pockets of crustal magnetism are scattered in clusters across the Martian surface, left in place by the global dynamo that once existed on the planet (Acuna et al., 1999). The strongest of these fields are concentrated in a complex found in the Southern hemisphere, while weaker field structures extend throughout equatorial latitudes. As the crustal magnetic fields interact with the incoming solar wind, they raise the height of Mars' magnetic boundaries (e.g., Brain et al., 2003; Edberg et al., 2008; Fang et al., 2017), alter the shape of the magnetotail (e.g., DiBraccio et al., 2018; Xu, Mitchell, Weber, et al., 2020), and reconnect with the IMF to form a dense network of magnetic topology (e.g., Brain, 2007; Weber et al., 2017; Xu et al., 2017).

The nonuniform distribution of crustal magnetic fields means that different regions of the planet are likely subject to very different magnetic field environments. As a result, the solar wind interaction with Mars is unlike any other in the solar system. Rather than an atmosphere that is shielded from the solar wind (as in the case of a global dipole) or one that is exposed (as in the case of fully unmagnetized planets like Venus), Mars represents a hybrid of the two situations. In some areas, crustal field structures provide shielding analogous to that of a global dynamo, with horizontal fields deflecting low-energy particles from the solar wind. Where these structures reconnect with the IMF, they create "cusps" of vertically oriented fields that may behave similarly to the polar outflow regions we observe at magnetized planets, channeling energy into localized pockets (e.g., Brain, 2007; Mitchell et al., 2001). And in the unmagnetized regions of Mars, the solar wind interacts directly with the top of the conducting ionosphere, creating a more typical induced magnetosphere. Additionally, the way any particular location on Mars interacts with the solar wind varies greatly as it rotates between the dayside and the nightside, as well as with changes in the incoming solar wind conditions (e.g., Brain et al., 2003, 2020; Weber et al., 2019, 2020). Crustal fields that are just strong enough to stand off the solar wind during typical conditions may be completely overpowered during periods of increased solar wind pressure. Relatedly, changes in solar wind pressure have also been shown to influence ion escape rates at Mars (Edberg et al., 2010; Nilsson et al., 2010; Ramstad, Barabash, Futaana, Nilsson, et al., 2017).

The overall influence that this system has on atmospheric escape is not immediately clear. The presence of magnetic shielding on a local scale would seem to inhibit escape to some degree, but the prevalence of energized cusp regions could do just as much to funnel enhanced escape through these channels (Brecht & Ledvina, 2014; Dubinin et al., 2020; Ma et al., 2014; Nilsson et al., 2011; Ramstad et al., 2016). Alternatively, it could be just as possible that the effects of the crustal magnetic fields are negligible when compared to the other sources of atmospheric escape at Mars, particularly when considering the planet's relatively weak gravitational pull. Photochemical escape, for example, accounts for the majority of present-day oxygen escape, while hydrogen leaves the planet through Jeans escape in number fluxes that dwarf those of other escape paths (Jakosky et al., 2018, and references within). In any case, further analysis of how the crustal fields affect atmospheric escape should be illuminating, both in constraining the evolution of Mars and in understanding how planetary magnetic fields affect atmospheric escape on a broader scale. This study presents the initial results of such an analysis.

Ion escape from Mars can occur through several different channels and processes, but all forms of ion escape involve the completion of three general conditions. First, ions must be created through the ionization of neutral atmospheric particles. Second, these ions need to be energized such that they reach escape energy. Third, the escaping ions must have a viable, unhindered path through which they can leave the system. In other words, the supply, energization, and transport of ions each play an important role in driving ion escape at Mars (Ramstad, Barabash, Futaana, Nilsson, & Holmström, 2017). Each of these steps could represent a bottleneck for escape under certain conditions. If the supply of ions through ionization is low, then escape rates will be low regardless of how much energy is delivered to the system. If many ions are created but energy input is low, then few will reach the velocities necessary to leave the planet. And even if many ions are brought to escape energy, they still might fail to be transported out of the system, perhaps due to the loss of energy through collisions or the presence of magnetic fields hindering their escape.

We use this three-step framework to analyze ion escape at Mars. Using data from the MAVEN spacecraft, we measure the supply, energization, and transport of ions in the Martian system. We interpret this information specifically in the context of how these processes are affected by the presence of crustal magnetic fields. We then use our measurements to estimate the extent to which crustal magnetic fields influence ion escape at Mars.

In Section 2, we discuss the data products and instruments used in this study. In section 3, we present results regarding the supply, energization, and transport of ions on the dayside of mars. In Section 4, we present comparable results for the Martian nightside. In Section 5, we link our dayside and nightside analyses together through a study of variations with solar zenith angle. In Section 6, we provide a condensed summary of our results thus far. In Section 7, we use the previous results to formulate estimates of crustal field influence on Martian ion escape. And in Section 8, we summarize our findings and discuss their associated implications.

2. Data and Instrumentation

This study uses ion densities and fluxes that were measured by the Suprathermal and Thermal Ion Composition (STATIC) instrument aboard MAVEN (McFadden et al., 2015). STATIC is an electrostatic analyzer that also makes use of time-of-flight analysis to measure ion fluxes across a range of masses (1–70 amu), energies (0.1 eV–20 keV), and look directions (360° by 90°). We use measurements from the instrument's D1 mode of operation, which samples particle distributions across 32 energy bins, 8 mass bins, and 64 directional bins with a time resolution of 16 s. This provides enough mass resolution to distinguish between O^+ and O_2^+ ions, while also providing a high enough angular resolution to determine particle flow directions. During MAVEN's orbit, STATIC adjusts its energy range based on the plasma populations it is sampling. Data in this study come from STATIC's upper ionosphere mode, which uses an energy range of 0.1–500 eV. Our analysis covers three and a half years of data, spanning from April 14, 2016 to September 2, 2019. During this time, MAVEN's orbit processed such that it had coverage across a range of latitudes, longitudes, and altitudes on both the dayside and the nightside of Mars. Data sampled below 200 km altitude are excluded from this study due to ion suppression issues that cause unreliable measurements in that region. We also exclude data taken above 1,000 km altitude, as we are primarily interested in the energization of particles in the upper ionosphere. Each individual STATIC measurement represents an instantaneous ion distribution function that is then corrected for both spacecraft velocity and spacecraft potential. Measurements of spacecraft potential are derived from a multi-instrument analysis technique that uses information from the Solar Wind Electron Analyzer (SWEA), STATIC, and the Langmuir Probe and Waves (LPW) instrument (e.g., Dong et al., 2017; Xu et al., 2018). For each D1 STATIC measurement of the ion distribution function, we take numerical moments to obtain ion densities and fluxes.

In this study, we also use measurements of vector magnetic field from the Magnetometer (MAG) (Connerney et al., 2015) and energetic electron fluxes from SWEA (Mitchell et al., 2016) to determine magnetic field topology using a method outlined in Xu et al. (2019). SWEA is a hemispheric electrostatic analyzer that covers a 360° by 120° field of view. Designed to measure electrons from both the ionosphere and the solar wind, it covers a range of energies from 3 eV to 4.6 keV. MAG is a fluxgate magnetometer that makes vector magnetic field measurements from 3 to 3,000 nT at a cadence of 32 Hz. Measurements from these two instruments are paired to produce an electron pitch-angle distribution (PAD) every 2 s. Using PADs and electron energy spectra, we have designed a method for identifying magnetic topology throughout the entire Martian system. This method analyzes (1) the presence of loss cones in electron PADs to determine when a field line is connected to the collisional atmosphere, (2) the presence of photoelectron energy signatures to determine when a field line is connected to the dayside ionosphere, (3) the presence of solar wind electron energy signatures to determine when a field line is connected to the IMF, and (4) the presence of suprathermal electron depletions to determine when a field line is located in a closed loop on the nightside of Mars. From these pieces of information, we are able to deduce whether a magnetic field line being measured by MAVEN is topologically open, closed, or draped, and we are also able to infer whether the field is connected to the dayside, the nightside, or both. For a complete explanation of our topology identification technique, see Sections 2.2 and 2.3 of Xu et al. (2019).

3. Dayside Results

We begin our analysis on the dayside of Mars, using measurements taken between 0° and 90° solar zenith angle.

3.1. Supply

In Figure 1 we present geographic maps of O_2^+ density across a range of altitudes on the dayside of Mars. As one would expect from a typical ionospheric profile, the density of O_2^+ decreases with altitude, and we can also see that at higher altitudes there are geographic variations in density that appear to correspond to crustal field locations. In the lowest altitude bin (200–288 km), O_2^+ densities are fairly uniform across the planet, but at the higher altitudes, we see that densities are largest in the southern hemisphere near 180° longitude (the middle of the plots), where the strongest crustal field regions are located.

Unfortunately, these maps suffer from relatively low data density. Many of the longitude-latitude bins contain only 10–20 points, and statistical noise seems fairly prevalent. However, in this study, we are less interested in distinguishing between specific crustal field structures than we are in understanding the general trends that separate magnetized and unmagnetized regions of Mars. To that end, Figures 2a–2d contain plots of ion density for both O_2^+ (panels a and b) and O^+ (panels c and d). In the left column, plots are a function of altitude and crustal magnetic field strength as modeled below the spacecraft location at a reference altitude of 150 km by the Morschauser model (Morschhauser et al., 2014). In the right column, plots are a function of altitude and magnetic elevation angle. For both O^+ and O_2^+ ions, we observe the same trend that was seen for O_2^+ ions in Figure 1. At low altitudes (near 200 km), ion densities of ~10^4 cm^{-3} are observed consistently across all magnetic field strengths. This is to be expected, as these ions are primarily created through photoionization, a process that is unaffected by local magnetic fields. Moving to higher altitudes, we can see O_2^+ densities decrease, and that this decrease is more gradual in regions of strong magnetic field. As a result, at any given altitude above 300 km, we observe higher ionospheric densities in crustal field regions than we do in unmagnetized regions of Mars. This result was previously observed using MARSIS radar soundings by Andrews et al. (2015), though that study was unable to make measurements below 350 km altitude. They suggested that the vertical fields associated with crustal field structures increase the transport of particles to the upper ionosphere, whereas ions in regions without crustal fields are constrained to low altitudes by horizontal induced magnetic fields. Our findings support this interpretation, and we suggest that in addition to transporting ionospheric plasma up to high altitudes, strong crustal fields are also likely able to effectively trap and recycle ions. Since collisions are unlikely above the exobase, many ions at this altitude will mirror within the field, remaining trapped in the crustal field structure until they are scattered into the loss cone or diffuse to high enough altitudes to encounter the solar wind. This leads to a build-up in density, as was reported by Lundin et al. (2011) and Nilsson et al. (2011). Those authors used *Mars Express* observations to make global maps of ion densities and fluxes, respectively, at Mars.

In panels a and c of Figure 2, we can also see a drop off in ion density that occurs at ~$500 - 600$ km altitude in weakly magnetized regions, rising up to ~1000 km altitude in strongly magnetized regions. This drop-off represents the transition region between the Martian ionosphere and shocked solar wind plasma. Over years of study, this boundary has been referred to by a bevy of different names, including the "ionopause," the "photoelectron boundary," or the "ionosphere boundary" (see Espley, 2018 for a full discussion of this terminology). These names each carry slightly different physical implications, so we will refer to this boundary region using the most general term of "ionosphere boundary" (IB). A few hundred kilometers above the IB lies a second boundary region, wherein the induced magnetic fields and thermal pressure of the ionosphere are at balance with the ram pressure of the solar wind. This boundary has also garnered a series of names over the years, but we will refer to it by the catch-all term "induced magnetosphere boundary" (IMB).

In Figures 2a and 2c, we see how crustal fields affect the altitude of the IB. Strong crustal fields deflect incoming sheath plasma at high altitudes, pushing the boundary further from Mars and allowing ionospheric plasma to extend up to 1,000 km altitude. This finding is in agreement with previous studies, several of which have found large asymmetries in boundary region altitudes between the strongly magnetized Southern hemisphere and the weakly magnetized Northern hemisphere (Crider et al., 2002; Fang et al., 2017;

Figure 1. Geographic maps of O_2^+ density on the dayside of Mars at nine different altitudes. Each panel has an *x*-axis of east longitude and a *y*-axis of latitude, binned with a spatial resolution of 9° × 9°. The altitude steps are linearly spaced between 200 km (upper left) and 1,000 km (lower right). Contours of crustal magnetic field strength (20 and 40 nT) as measured by Mars Global Surveyor at 400 km altitude are overlaid in white for context. Bins with fewer than 10 points are colored gray.
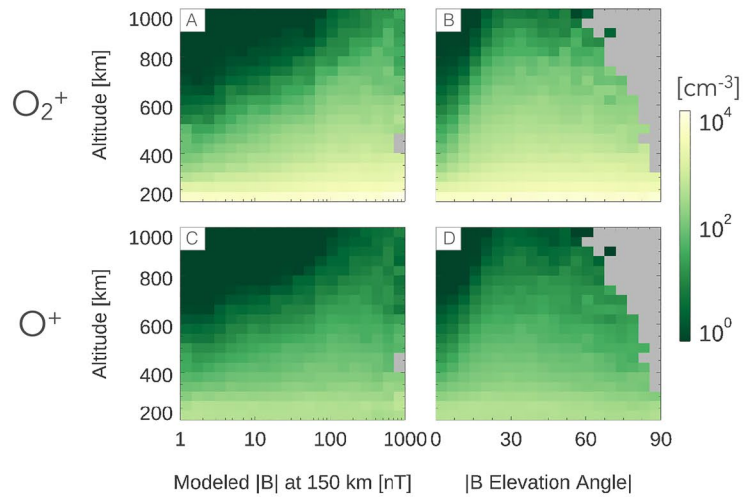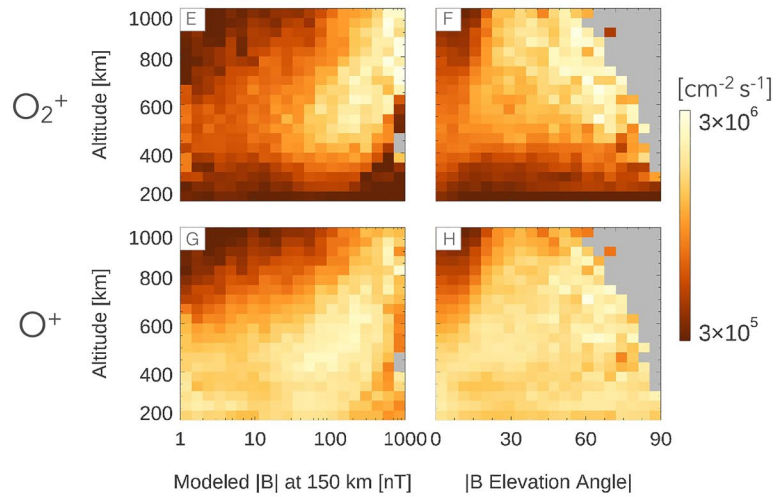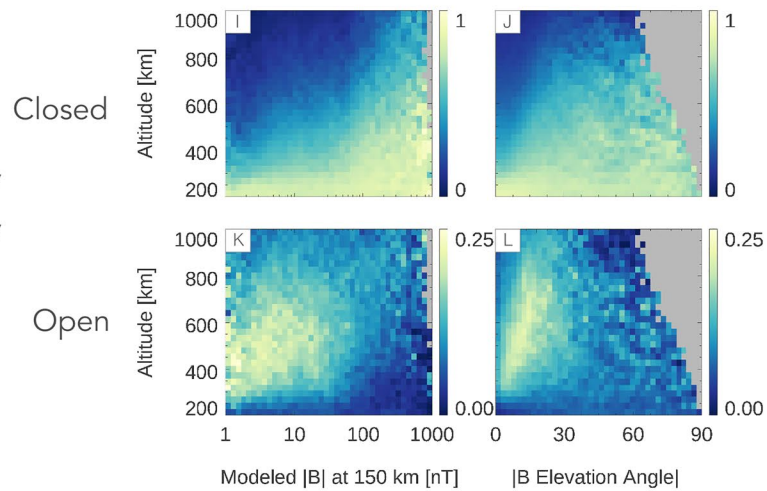
Figure 2.

Matsunaga et al., 2017; Mitchell et al., 2001). A similar result was also reported by Brain et al. (2003), who showed that these variations also occur on a local scale around crustal field structures.

Figures 2b and 2d will be used as a point of reference for future discussion. For now, they show that at low altitudes dayside ion density is independent of field line geometry. Further, the depletion in the upper left corner of these plots is also due to the IMB, as horizontal fields above 600 km altitude are dominated by draped fields in the magnetosheath.

Overall, we find that the dayside supply of ions at mars is consistently large at low altitudes, and that this supply extends to higher altitudes in crustal field regions. Whether the ion supply is effectively energized and transported away from Mars will be investigated in the next sections.

3.2. Energy

To study where ions at Mars gain enough energy to escape the planet, we present Figures 2e–2h. Using the same axes and organization as panels a through d, these plots contain measurements of the flux of ions traveling upward with energy greater than escape energy on the dayside of Mars. Since escape energy varies with altitude, it is calculated at the spacecraft location for each measurement. Across the altitude range, we are studying, O^+ escape energy varies from 2 eV (at 200 km) to 1.62 eV (at 1,000 km), while O_2^+ escape energy varies from 4 to 3.26 eV. In the top left of each of the four panels, we again see the effects of the IB. Fluxes of ionospheric particles are primarily found below the IB, as the sheath plasma located above is composed primarily of protons. If we compare the IB as mapped out in Figures 2a–2d to what we see in Figures 2e–2h, we find small fluxes of energetic ions extending out past the boundary and into the far upper-left corner of the plot. Ions that make it to these altitudes are a primary source for ion pickup, and are all likely to escape the system provided that they do not collide with the Martian atmosphere as they are carried away by the solar wind.

Below the IB, we find high fluxes of energetic ions, and we observe differences in the energization of O^+ and O_2^+. O^+ ions reach escape energy fairly uniformly across all crustal field strengths, and appear to typically be sufficiently energized even at our lowest sampled altitude of 200 km. This means that very quickly upon reaching the exobase, O^+ is accelerated to escape energy. We do not identify a definite source for this energization, but suggest that much of it is likely due to field-aligned electric potentials, which have been measured throughout the Martian ionosphere. Xu et al. (2018) and Collinson et al. (2019) used electron energy spectra measured by MAVEN to infer the magnitude of field-aligned potentials at Mars, determining that potential drops on the order of -1.0 to -1.5 V exist around the planet. The authors of those studies did not distinguish between source mechanisms, but suggested that ambipolar electric fields are likely the primary driver. The ambipolar fields were found to be strongest near the ion exobase, where they could play a role in pulling ions out of the collisional atmosphere and toward escape. Here, we potentially see the result of this process, with O^+ traveling upwards at escape energy across the planet.

At 200 km altitude in Figures 2e and 2f, outward fluxes of O_2^+ ions with escape energy are comparatively low. At ~300–400 km altitude, however, we begin to find higher fluxes of escaping ions, suggesting that this is the altitude at which the ions are predominantly reaching escape energy. It makes intuitive sense that O_2^+ ions would need to be accelerated over a larger distance than O^+ ions to reach escape energy, as their escape energy is twice as large. Further, a 1.5 V field-aligned potential drop alone is unable to provide the ~4 eV required for O_2^+ escape. However, Ergun et al. (2016) found that ions gain energy through plasma waves and other heating mechanisms after being lofted past the exobase, and that even a moderate potential drop of ~0.5 eV is sufficient to bring them to this altitude. We suggest that such a process is likely happening here, and that these heating mechanisms are able to bring O^+ to escape energy more quickly than O_2^+ upon their motion to higher altitudes.

Figure 2. Three sets of plots containing results from the dayside of Mars (SZA 0°–90°). (a–d): Density of O_2^+ and O^+ ions. (e–h): Flux of O_2^+ and O^+ ions traveling upward with energy in excess of the local escape energy for that ion. (i–l): Frequency of observing closed and open magnetic topologies. In the left column, plots are a function of altitude and crustal magnetic field strength as modeled at a reference altitude of 150 km by the Morschhauser model (Morschhauser et al., 2014). In the right column, plots are a function of altitude and the absolute value of magnetic elevation angle, from 0° (horizontal fields) to 90° (vertical fields). Bins with fewer than 50 points are colored gray.

In Figure 2e, we also find that O_2^+ fluxes vary substantially with crustal field strength. Specifically, fluxes in crustal field regions (>20 nT) are higher than those in the unmagnetized regions, and the altitude at which this flux enhancement occurs moves upward with increased crustal field strength. In the strongest crustal field regions (500–1,000 nT), peak energetic O_2^+ fluxes are found near 1,000 km altitude, just below where these crustal fields stand off with the solar wind. For the more middling strength crustal fields (~50 nT), peak fluxes are found at 500 km altitude, just below where these fields interface with the IB. In general, we find that the loop-tops and outer edges of crustal field structures show enhanced ion fluxes, while the inner, low-altitude sections of crustal field structures remain comparatively unenergized.

The resulting situation looks somewhat similar to that of electrons trapped in crustal fields on the nightside of Mars. In that circumstance, the outer edges of crustal field structures are filled with mirroring energetic electrons, while the inner sections are severely depleted of particles (e.g., Mitchell et al., 2001; Steckiewicz et al., 2017). In the case we observe on the dayside of Mars, a strong supply of ions exists throughout the entire crustal field structure (as seen in Figure 2a), but on the outer edges, the particles are much more energetic and more likely to reach escape energy. We suggest two possible causes for this trend. First, it may be that only the high-energy tail of particles found within the crustal fields are able to diffuse upward to the outer edges, while low-energy ions bound to the central loops of a field structure are confined to stay there. Second, particles that reach the outer edges of crustal field structures are more likely to absorb energy from the incoming solar wind. That is, crustal field loop-tops interface directly with shocked solar wind plasma, and particles located at these loop tops may be susceptible to energization via plasma waves (e.g., Ergun et al., 2006), magnetic pumping (e.g., Fowler et al., 2020; Lundin & Hultqvist, 1989), or other such heating mechanisms. The true cause may, of course, be a combination of these two hypotheses. Upon close inspection, a similar enhancement can be seen in the O^+ fluxes in Figure 2g, though it is less exaggerated due to the generally higher fluxes exhibited by that particle species.

In addition to the heating mechanisms mentioned above, some fraction of the flux we observe in strong crustal field regions was likely accelerated by the large field-aligned potentials that have been observed in crustal field cusps. Cusp potential drops in excess of 100 V (much stronger than the typical 1–2 V ambipolar potentials found across the planet) have been reported by several studies (Dubinin et al., 2008; Lundin et al., 2006), including a recent work that found such potential structures in association with observations of discrete aurora (Xu, Mitchell, McFadden, et al., 2020). These field-aligned potentials should be able to bring oxygen ions far above escape energy, driving large fluxes as they do. However, it is currently unclear how frequently potentials of this magnitude occur at Mars, so we do not speculate on the extent to which they are responsible for the ion fluxes shown in Figures 2e–2h. We expect, however, that most of the escape flux driven in this way would be located on more vertically oriented crustal field cusps. This is observed as a flux enhancement at high altitudes and high elevation angles in the upper right of Figure 2f. While we have few measurements in this region of parameter space, the measurements we do have are some of the highest O_2^+ fluxes we observe on the dayside, despite this region hosting comparatively low O_2^+ densities in Figure 2b. This suggests that the particles traveling through this region are very highly energized. A quick calculation using the flux and density of escaping ions in this region finds energies on the order of 100 eV.

In summary, ion energization is present across the dayside of Mars, but is strongest in the crustal field regions. Ions in non-crustal field regions (of which there is a large supply) are comparatively unenergized, suggesting that dayside escape is at least partially energy-limited. Whether the strong fluxes we observe in crustal field regions are effectively transported from the system is investigated in the next section.

3.3. Transport

With maps of energetic ion fluxes in hand, we next use calculations of magnetic topology to analyze whether these particles are likely to escape. Figures 2i–2l contain plots of the frequency of observing specified field topologies on the dayside of Mars. The values in each bin range from 0 to 1, representing the fraction of observations in that bin that were of the specified topology. A value of 0 therefore means that the specified topology is observed 0% of the time, while 1 means that the specified topology is observed 100% of the time. Plots are organized using the same axes as in the previous panels, but in this case, the rows correspond to closed and open field topology, rather than to different particle species. We identify when magnetic field lines being measured by MAVEN are connected to the Martian atmosphere at both ends ("closed"),

connected to both the Martian atmosphere and the solar wind ("open"), or connected only to the solar wind ("draped," not shown here). As stated previously, our method of topological analysis is described in full detail in Xu et al. (2019).

On the dayside, closed fields are more common at lower altitudes and in strong crustal field regions. In fact, at our lowest studied altitude of 200 km, fields are almost uniformly closed across the dayside. This is a somewhat surprising result that was initially outlined by Xu et al. (2017). In interpreting this finding, it may be important to recall that our method of identifying topology determines whether field lines are connected to the collisional atmosphere, rather than to crustal field sources locked in the planet's surface. This means that many of the closed fields we observe at 200 km may truly be draped or induced field lines that thread through the collisional atmosphere multiple times. When we sample a field line of this kind while between its two points of connectivity, we observe a field that is, closed in the context of electron transport. At higher altitudes, we would expect that it would become more common for these draped and induced fields to only thread through the atmosphere once, causing an increase in open field topology. This feature is present in Figures 2i and 2k. We observe a transition region located between 300 and 600 km where open field topology becomes more frequent and closed topology becomes less frequent. The altitude at which this transition occurs increases with increasing field strength, and by comparing this to our previous analysis of the IB location we find that open field lines are found predominantly in an altitude band located between the IB and low-altitude closed fields. This transition region is also where oxygen ion fluxes above escape energy reach their peak values in Figures 2e and 2g, suggesting that many of the energized ions should have a direct path along open field lines through which they can escape. Closed topology, however, still remains dominant in this region, with 50% or more of the measured field lines being closed.

Thus far we have been using magnetic topology as a determination of where ions can travel. However, our calculations of topology were made using electrons, and will not apply to energetic ion fluxes in all situations. We therefore need to determine how readily our definitions of "closed" and "open" truly apply to ions at this energy. Depending on the extent to which ion fluxes we measure are frozen onto the local magnetic field, the fraction of ions that are escaping could vary substantially.

To determine whether gyrating charged particles are effectively bound to a magnetic field, we take a commonly used comparison between the particle gyroradius and the length-scale of the local magnetic field field. Following the methods of several previous studies, we calculate R_g/L, where R_g is the ion gyroradius ($mv_\perp / |q| B$) and L is a characteristic magnetic length scale given by $|B| / |\nabla B|$ (Büchner & Zelenyi, 1989; Zhang et al., 2016). We calculate the gradient of the magnetic field (∇B) using statistically averaged maps of the magnetic field, as measured by MAVEN's MAG instrument over five years of data. We then used the magnetic field magnitude to calculate the local gyroradius of an O_2^+ ion at escape energy (~4 eV). This calculation assumed an average particle pitch angle of 45° (an arbitrary intermediate pitch angle). We then estimate particle magnetization as R_g/L. Values much less than 1 suggest that a particle is likely to follow magnetic field lines closely, often referred to as "magnetized," while values much greater than 1 suggest a particle is only weakly bound to the magnetic field, or "unmagnetized." Additional details of this method are included in the supplementary materials of this study.

In Figure 3, we present our calculations of O_2^+ magnetization as a function of altitude, magnetic field strength, and magnetic elevation angle. Before comparing these plots to those made in previous sections, we should first address several caveats associated with this calculation. First, our analysis has only accounted for spatial variations in magnetic fields. Magnetic fields also vary in time, potentially quickly enough that any trapped ion might encounter different field topologies over the course of one 10–50 s bounce period. Second, we did not account for electric fields at all in this analysis, which in many circumstances are just as important if not more important than magnetic fields in the context of driving ion motion at Mars. Third, our calculation of gyroradius assumed the particles to have exactly escape energy, when in reality many of the fluxes we have observed were of higher energy than this by more than a factor of 2. Each of these three caveats has the effect of making particles less magnetized than we calculate. This means that we should treat these plots as representing a lower bound to R_g/L (or as an upper bound to the extent to which these ions are magnetized).
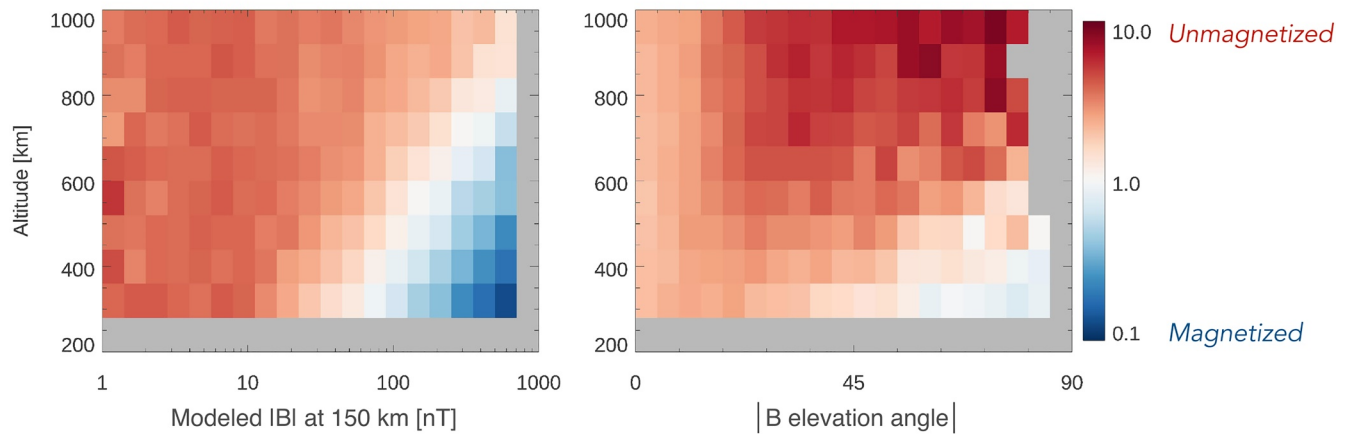
Figure 3. Magnetization of O_2^+ ions at escape energy, calculated through a comparison between ion gyroradius and the length scale of the local magnetic field. The figure on the left plots magnetization as a function of altitude and modeled magnetic field strength. The figure on the right plots magnetization as a function of altitude and local elevation angle, from 0° (horizontal fields) to 90° (vertical fields). Bins with fewer than 50 points are shaded gray.

With this in mind, Figure 3 illustrates that only in the strongest crustal field regions and at low altitudes are O_2^+ particles at escape energy effectively magnetized. This means that much of the flux that we analyzed in Figures 2e–2h may be able to escape Mars, even if found on a topologically closed field line. This is not to say that field topology makes no difference—closed field lines are still likely to disrupt ion flows and impede escape—but particles are only truly frozen onto their local magnetic field in the center of strong crustal field structures. At the tops of these structures, the magnetic field becomes weak enough that particles are only slightly magnetized, if at all. More specifically, the band of white extending from 100 nT and 300 km altitude to 1,000 nT and 800 km altitude signifies the transition to unmagnetized particles.

In summary, we find that open fields are present in the regions where dayside ion energization is strongest, and should therefore be able to transport some fraction of these particles. What fractions are actually transported to escaping is difficult to determine, due both to the presence of many closed fields and the ions being relatively unmagnetized. We therefore will need to consider a range of possible transport efficiencies when making estimates of total ion escape later in this study.

4. Nightside Results

Turning to the nightside of Mars, we next present Figure 4 using the same format as Figure 2. As in the previous section, we analyze ion density, ion flux, and magnetic topology, but this time we only use data sampled at solar zenith angles greater than 120°.

4.1. Supply

In Figure 4a–4d, we plot O^+ and O_2^+ densities on the nightside of Mars, where the supply of ions has a very different structure than on the dayside. Note that these plots use a different color scale than those investigating the dayside in Figure 2; plasma densities are several orders of magnitude lower on the nightside. Immediately it is apparent that these plots show a much weaker dependence on altitude. Across the full altitude range, nightside densities vary only from ~10 to 60 cm^{-3} for O_2^+ and from ~1 to 5 cm^{-3} for O^+, as compared to the several orders of magnitude variation observed on the dayside. This ionospheric structure is in agreement with Fowler et al. (2015), who showed that above 200 km nightside electron densities measured by LPW are roughly constant with altitude. That study also showed that a modest nightside ionosphere is sustained at low altitudes (<200 km) by precipitating electrons. Though our observations are unable to extend to such low altitudes, the edge of this feature is found at the bottom of our O_2^+ plots. Near 200 km in panels (a) and (b) we see a slight enhancement in O_2^+ density as compared to higher altitudes, and
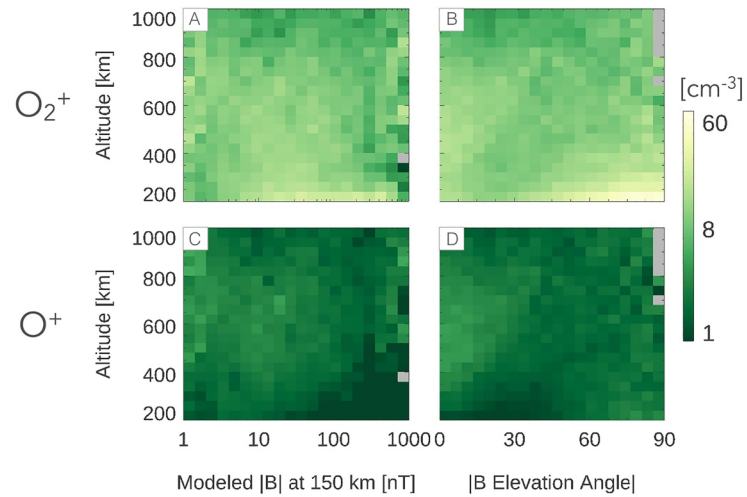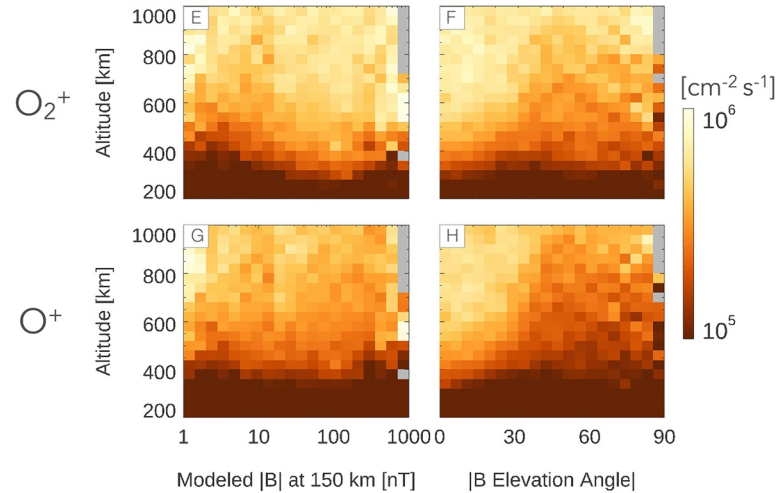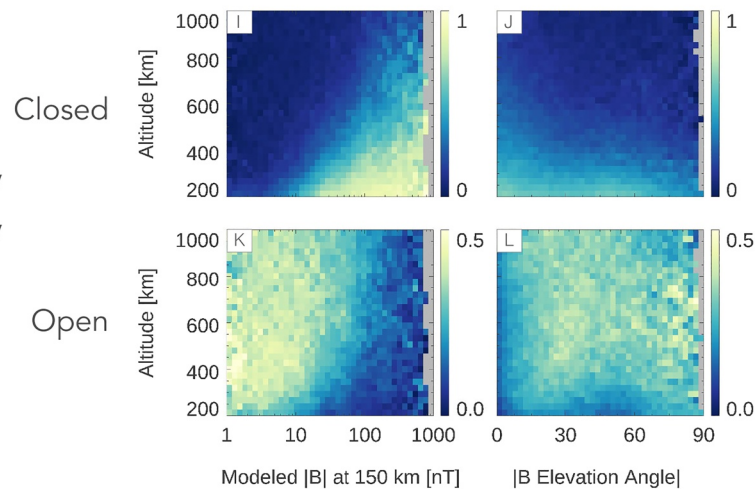
Figure 4. Three sets of plots containing results from the nightside of Mars (SZA 120°–180°). (a–d): Density of O_2^+ and O^+ ions. (e–h): Flux of O_2^+ and O^+ ions traveling upward with energy in excess of the local escape energy for that ion. (i–l): Frequency of observing closed and open magnetic topologies. Plots and axes are organized in the same manner as in Figure 2.

from panel (b) it seems that this enhancement is most prominent on vertically oriented fields. These fields (particularly those associated with crustal field cusp regions) are the most likely to facilitate precipitation of electrons into the nightside atmosphere, and here we observe traces of the resulting production of ions through impact ionization.

Figures 4a–4d illustrate that the nightside of Mars has a sparse and tenuous ion population, with low densities of ions extending fairly uniformly to high altitudes. The lack of any incoming solar wind ram pressure on this side of the planet means that particles are not compressed down to low altitudes as severely as on the dayside. The relatively weak ionization source, however, means that ion densities remain low across all altitudes, particularly above the exobase (Fowler et al., 2015; Fox et al., 1993).

We should note that although these observations are taken on the nightside of Mars, the ions that we measure at high altitudes did not necessarily originate in the nightside ionosphere. As ions flow away from Mars, they are pushed in the antisolar direction by the solar wind. Particles from the dayside frequently flow around Mars and into the nightside magnetotail, traveling along the flanks of Mars's geometric shadow (Frahm et al., 2006; Liemohn et al., 2007). There are signatures of this flow in Figure 4, particularly in panels (b) and (d). These plots show enhanced densities at low altitude and high elevation angle due to electron precipitation along vertical fields, reaching 60 cm^{-3} for O$_2^+$ and 5 cm^{-3} for O$^+$. But there is also a separate slight enhancement found along the left sides of these plots. Moving to higher altitudes, this enhancement can be found at steeper and steeper elevation angles. This geometry corresponds to magnetic fields that drape around the planet and extend directly down the magnetotail, many of which carry ions flowing from the dayside. At low altitudes near the terminator, draped fields are nearly horizontal to the planet, but as they extend downtail they become increasingly vertical relative to the surface below them, resulting in the observed trend with altitude. Ion densities on these field lines do not appear to be appreciably larger than they are throughout the rest of the nightside.

Overall, the supply of ions on the nightside of Mars is much lower than on the dayside, and shows only slight variation with crustal magnetic field strength. As with our dayside analysis, we will next investigate the energization and transport of this supply.

4.2. Energy

As shown in Figures 4e–4h, fluxes of escaping O$^+$ and O$_2^+$ ions on the nightside of Mars display very similar behavior. At low altitudes, fluxes at escape energy are low, despite the O$_2^+$ density enhancement due to precipitating electrons that was observed in Figures 4a–4d. Moving to higher altitudes, particles are eventually accelerated to escape energy, and by 300–400 km altitude we see an increase in escaping fluxes at all crustal field strengths. In strong crustal field regions, O$_2^+$ escape fluxes begin to increase at a lower altitude than in the non-crustal field regions, likely due to the aforementioned higher supply found in those locations.

As on the dayside, many escaping oxygen ions are likely accelerated via ambipolar electric fields. Since there is no standoff with the solar wind on this side of the planet, upward traveling ions that reach escape energy are able to flow downtail unimpeded, creating a steady flow of ions up through our highest analyzed altitude of 1,000 km. Just as in our plots of nightside ion density (Figures 4a–4d), little variation is seen with crustal field strength. On the left-hand side of Figures 4f and 4h, we see an enhancement of flux that moves to higher elevation angles as it reaches higher altitudes. This is the same signature of dayside ion fluxes flowing tailward through the nightside that was noted previously in Figure 4b. These fluxes are carried on magnetic field lines connected to the dayside ionosphere that stretch directly downtail. Modeling studies have suggested that this may be an important pathway for ion escape (Liemohn et al., 2007). By comparing the left and right sides of Figure 4f, we can make a direct comparison between fluxes sourced from the dayside and the nightside of Mars, respectively. For both O$^+$ and O$_2^+$, the fluxes coming from the dayside appear to be stronger by roughly half an order of magnitude. This is in agreement with previous maps made using *Mars Express* measurements of high-energy ion fluxes (Nilsson et al., 2011). Our analysis extends this result to include particles that have only just reached escape energy.

To summarize, nightside ion energization occurs across all crustal magnetic field strengths, above any regions where there are notable ion densities. This suggests that nightside ion escape is limited by supply, and

that if more ions were created they would likely be energized as well. Energized ion fluxes are much lower on the nightside than on the dayside, likely due to the low supply of ions.

4.3. Transport

In Figures 4i–4l, we present plots of the frequency of observing specified field topologies on the nightside of Mars. In these figures, we find somewhat similar trends to those we observed on the dayside. Closed fields are found most frequently at low altitudes and in strong crustal field regions, while open fields are more common in weakly magnetized regions and at higher altitudes. Unlike on the dayside, open fields are found down through the exobase, particularly in weakly magnetized regions, and they also freely extend out through 1,000 km altitude. Additionally, Figure 4l allows us to identify two separate populations of open field lines. At low altitudes, we find one grouping of open field lines at near-horizontal elevation angles (0°), and a separate grouping of open field lines found at near-vertical elevation angles (90°). Separating these two features is a decrease in open topology frequency found at intermediate pitch angles (45°). As discussed in the previous two sections, these correspond to open fields connected to the dayside and the nightside of the planet, respectively. Escaping ion fluxes corresponding to both of these populations can be found in Figure 4h.

It therefore appears that open field lines are available for the transport of most of the energized ions found in Figures 4e–4h, suggesting again that nightside escape is likely supply limited.

5. Trends With Solar Zenith Angle

To link together our dayside and nightside analyses, we next present a set of plots that describe the supply, energization, and transport of oxygen ions as a function of altitude and solar zenith angle. This is shown in Figure 5. In each panel, we have plotted dotted lines showing standard locations of the IB and IMB as modeled by Ramstad, Barabash, Futaana, & Holmström (2017), and have also included a line marking the geometric shadow of Mars. In this figure, we observe a few noteworthy features. Densities and fluxes (top and middle rows) are higher on the dayside (0–90° SZA) than on the nightside (90–180° SZA) by an order of magnitude or more. We can see the IB in the form of a steep ion density gradient (top plots), and as in our dayside analysis, we find that just below the IB lies a region of increased flux (middle plots) and open field lines (bottom plots) that could potentially facilitate escape. As expected, the IB and IMB are closest to the planet at the subsolar point, flaring out at the planet's flanks. Finally, we can again see that densities, fluxes, and open field lines on the nightside all extend through the entirety of our sampled altitude range. This includes a band of enhanced ion density (top plots) and flux (middle plots) that begins at 90° SZA and 200 km altitude, curving upwards and reaching 1,000 km altitude at ~120° SZA. This maps very closely with the edge of the planet's geometric shadow, as shown by the dotted line. We can interpret this band as representing dayside ions flowing around the planet and downtail on the nightside.

6. Interpretation

The information provided in the preceding sections is summarized in the following main points:

1. At low altitudes on the dayside, ion densities are uniformly high. Crustal field regions allow for the transport of these particles to higher altitudes, leading to local enhancements in density and flux. The escape of ions on the dayside therefore appears to be limited by energization and transport, rather than by supply.
2. Below the IMB and above the tops of crustal field structures, there is an interaction region where dayside ions readily gain escape energy. This region also marks a transition to increased open magnetic field topology.
3. On the nightside, particles flow away from the planet more freely than on the dayside, with escape fluxes appearing wherever there are notable ion densities. This suggests that the escape of ions on the nightside is limited by supply.
4. Overall, escape fluxes from the nightside ionosphere appear to be significantly lower than those from the dayside ionosphere.
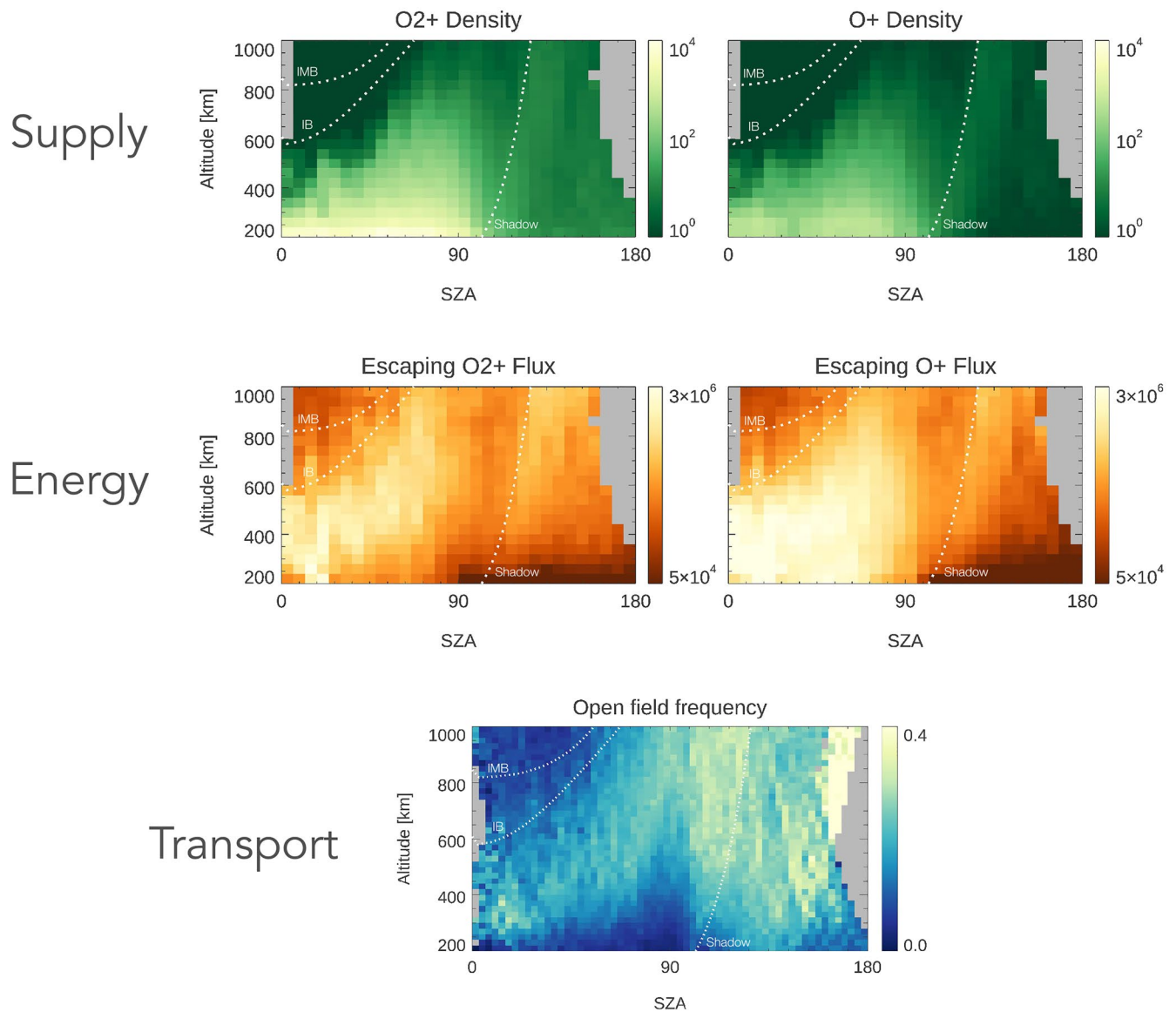
Figure 5. As a function of altitude and solar zenith angle, the supply, energization, and transport of O_2^+ and O^+ ions at Mars. The top row contains plots of ion density (cm^{-2}). The middle row contains plots of ion fluxes traveling upward with escape energy ($cm^{-2}\,s^{-1}$). The bottom plot shows the observation frequency of open field topology around Mars. In each panel, dotted lines show modeled locations of the IMB and IB, as well as the geometric shadow of Mars. Bins containing fewer than 50 points are colored gray.

5. Oxygen ions at escape energy are only strongly magnetized in strong crustal field regions at low altitudes. In regions of Mars containing no crustal fields, oxygen ions are only weakly affected by local field topology.

7. Estimates of Crustal Field Contribution to Ion Escape

The primary goal of this study is to use in-situ spacecraft measurements to constrain how crustal magnetic fields influence ion escape at Mars. We next present two calculations toward that end. The first is an estimate of the net effect that crustal magnetic fields have on global ion escape at Mars. The second is an estimate of the net effect caused by a single crustal field structure on ion escape in its local environment.

7.1. Effect of Crustal Magnetic Fields on Dayside Ion Escape

In Figures 2e and 2g, we showed measurements of upward traveling ion flux above escape energy. Combining these measurements with our knowledge of topology and particle magnetization, we can construct a rough estimate of how crustal fields influence ion escape at Mars. For the purposes of this calculation, we divide the crustal magnetic fields of Mars into three groupings: weak fields (0–20 nT), medium fields (20–100 nT), and strong fields (100–1,000 nT), where the nT values given here correspond to modeled field strength at 150 km (the *x*-axis in Figures 2e and 2g). For each of these groupings, we will calculate an estimate of ion outflow using measurements of fluxes, topology, magnetization, and the total surface area covered by that strength field. In making these calculations, we focus on the dayside of Mars, as escape rates on the dayside are 5–10 times higher than on the nightside (see Figures 2e–2h and 4e)–4h).

From Figure 3, we know that energetic ions found in weak field regions are substantially unmagnetized. We therefore take all of the upward flux measured at escape energy in those regions as successfully escaping the planet. Focusing on O_2^+ initially, we use fluxes measured between 400 and 600 km altitude for weak field regions, as this is the altitude range at which we observe ions typically reaching escape energy in Figure 2e. We find typical O_2^+ fluxes for weak field regions to be ~6.5×10^5 cm^{-2} s^{-1}. For medium and strong field regions, we assume that particle escape is occurring near the top of crustal field structures, in the region of peak energization and increased open topology that we discussed in previous sections. For medium strength fields, this corresponds to an altitude of 400–700 km, while for strong fields it corresponds to an altitude of 600–1,000 km. In each of these regions, we assume that any upward flux measured at or above escape energy on an open field line is escaping. Flux measured at this energy on a closed field line, however, we take to only potentially be escaping, as Figure 3 suggests that these particles are still partially magnetized. To account for this, we assign each region a scale factor (α for medium fields, and β for strong fields) representing the fraction of escape energy flux on closed field lines that succeeds in escaping the planet. Combining the crustal field groupings, we then calculate total escape as:

$$
\begin{aligned}
\text{Total Escape} =\ & F_1 A_1 \\
& + F_2^{open} A_2^{open} + \alpha F_2^{closed} A_2^{closed} \\
& + F_3^{open} A_3^{open} + \beta F_3^{closed} A_3^{closed}
\end{aligned}
\tag{1}
$$

Here, the subscripts 1, 2, and 3 correspond to weak, medium, and strong fields, respectively. The superscripts *open* and *closed* specify the measured field topology. F represents ion flux, and A represents the area covered by fields of the specified strength. For example, A_2^{open} represents the area covered by medium strength fields with open topology, while A_3^{closed} represents the area covered by strong fields with closed topology. We determine the area covered by each crustal field strength by averaging the Morschauser model field onto a grid of 0.5° longitude × 0.5° latitude bins and then calculating the total area covered by bins corresponding to each strength range. Finally, α and β are the factors that determine what fraction of flux found on closed topology escapes in medium and strong fields, respectively.

Results of this calculation are shown in Figure 6a, which provides O_2^+ escape rates as a function of α and β. We can see in this figure that even with $\alpha = 0$ and $\beta = 0$, we find an ion escape rate larger than 7×10^{23} s^{-1}. This encompasses all escape occurring in weak field regions and on open field lines in medium and strong field regions. If we increase α from 0 to 1, effectively assuming that all ion flux at escape energy in medium strength field regions will escape, this raises the ion escape by a factor of 1.5 to 1.1×10^{24} s^{-1}. From here, increasing β from 0 to 1 (assuming that all flux at escape energy in strong field regions escapes the planet) raises the total ion escape to 1.3×10^{24} s^{-1}, a factor of 1.2 increase. This last increase in particular is a relatively small effect. This is due to the fact that strong crustal fields as we define them only make up ~10% of the Martian surface.

To estimate the net effect of crustal magnetic fields, we can now compare these results to the escape rate that would result if the planet was only subject to our "weak field" regions, as these regions tend to be dominated by induced magnetic fields. That is, we calculate $F_1 A_{total}$, a quantity that is, plotted in Figure 6 as a horizontal dashed line. In this estimation, we see that ion escape is only increased by the presence of crustal fields if α and β are both close to one. This seems unlikely, as this would mean that magnetic fields present virtually no obstacle to escaping ions at Mars. Previous modeling studies have found that the presence of
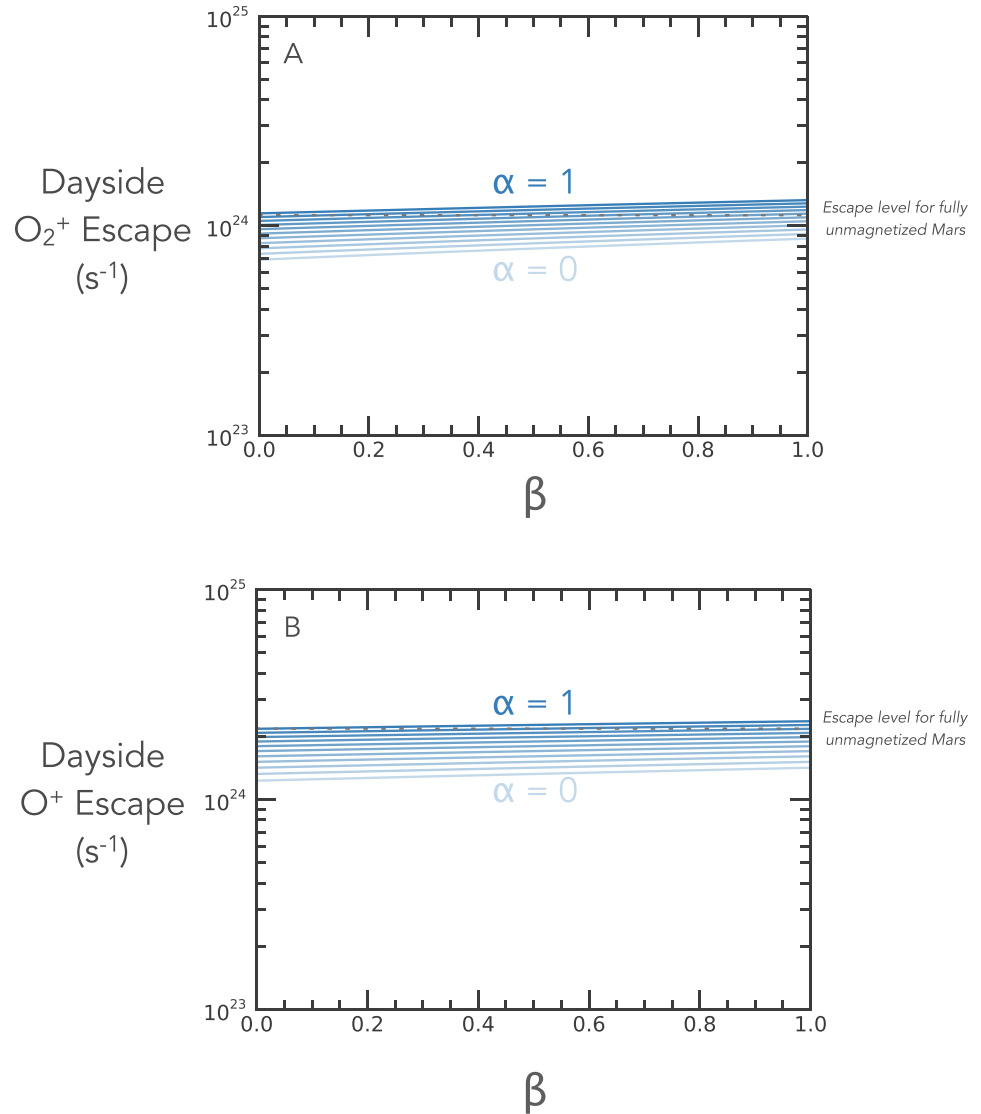
Figure 6. Dayside ion escape at Mars calculated through Equation 1. α represents the fraction of upward flux on medium strength closed fields that escapes, while β represents the fraction of upward flux on high strength closed fields that escapes. The horizontal dotted lines correspond to the escape rates that result from applying fluxes found in the low-strength field regions to the total area of Mars.

crustal fields decreases ion escape at Mars by roughly 20% (Fang et al., 2010, 2015; Ma et al., 2014). We find a comparable decrease in ion escape if we assume more conservative (though arbitrary) values of $\alpha = 0.5$ and $\beta = 0.2$. This results in an O_2^+ escape rate of $\sim 9 \times 10^{23}$ s^{-1}.

Repeating the process described above for O^+ escape results in Figure 6b. The trends exhibited are almost identical, but with escape rates that are uniformly higher by a factor of $\sim$2. We find that escape is only raised above that of an unmagnetized Mars if α and β are both close to one. In the case used above of $\alpha = 0.5$, $\beta = 0.2$, escape is decreased by 30% from the unmagnetized case. Note that in this calculation we have only considered escape from the dayside of Mars. Repeating these calculations for the nightside of Mars results in escape rates of roughly 10^{23} s^{-1}, an order of magnitude lower than the dayside.

7.2. Effect of a Crustal Field Structure on Local Ion Escape

Using a similar framework as in the previous estimate, we now calculate the net effect that a crustal field structure has on local ion flux. This amounts to a simple comparison of the escape fluxes calculated in weak, medium, and strong field regions, without accounting for the total area of Mars covered by these fields. In weak field regions, the total escape flux of O_2^+ and O^+ has a median value of 1.9×10^6 cm^{-2} s^{-1}. In medium-strength field regions, escape flux varies with our assumed value of α from 0.4×10^6 cm^{-2} s^{-1} ($\alpha = 0$) to 2.8×10^6 cm^{-2} s^{-1} ($\alpha = 1$). This range spans from an 80% decrease to a 50% increase from the weak field regions, depending on the assumed magnetization. For a medium-strength crustal field region to have the same escape flux as a weak crustal field region, an α value of 0.65 would be required, implying that 65% of all flux on closed field lines would need to escape the planet. In high-strength crustal field regions, escape fluxes range from 0.3×10^6 cm^{-2} s^{-1} ($\beta = 0$) to 2.9×10^6 cm^{-2} s^{-1} ($\beta = 1$). To achieve the same escape flux as a weak field region, 60% of the flux measured on closed field lines would need to escape the planet ($\beta = 0.6$). This suggests that escaping ions would need to be very unmagnetized in order for the presence of crustal fields to increase local ion escape.

8. Conclusion

In this study, we used data from the MAVEN spacecraft to investigate the effects of crustal magnetic fields on ion escape at Mars. We analyzed the supply of ions using maps of ion density, the energization of ions using maps of ion flux at escape energy, and the possible transport of ions using maps of magnetic field topology. We used magnetic field data from MAVEN to make maps of particle magnetization in crustal magnetic fields, allowing us to gauge the extent to which escaping ions are affected by magnetic topology.

Together, these works provided us with an understanding of ion escape at Mars that we then used to estimate the net effect that crustal magnetic fields have on Martian ion escape. The results of this estimate are shown in Figure 6, where we determined that the presence of crustal fields affects global ion escape by less than a factor of 2. Depending on the assumptions one makes regarding how effectively particles can escape from closed field lines, the influence of crustal magnetic fields could range from a net decrease in escape of 40% to a net increase of 20%. Under fairly typical assumptions, it seems likely that crustal fields currently decrease global ion escape by 20%–30%, a finding that is in agreement with previous modeling results.

In this calculation, we did not account at all for the effects of upstream drivers, but it is likely that escape from crustal field regions is significantly impacted by solar wind conditions. Weber et al. (2019), for example, showed that increased solar wind pressure tends to compress crustal fields on the dayside of Mars, leaving the ionosphere more exposed. If solar wind variations occur on a fast enough timescale, it is possible that this could leave the high ion densities found in crustal field regions suddenly exposed to the solar wind, leading to a large increase in ion outflow. This may contribute to the 10× enhancement in ion escape that Jakosky, Grebowsky, et al. (2015) observed during the impact of an interplanetary coronal mass ejection at Mars.

Finally, we estimated the effect that crustal field structures have on local ion escape, ignoring the global distribution of fields. We found that both medium-strength and strong crustal field regions could potentially increase local ion escape, but only if the ions were sufficiently unmagnetized that over 60% of ions found on closed magnetic fields with escape energy succeed in escaping. If ions with escape energy are not unmagnetized to this degree, then crustal fields should be taken to decrease local escape. In the future, the use of numerical models could help refine this result further. Test-particle models, for example, could provide a more exact determination of particle magnetization in the Martian crustal magnetic fields, allowing us to make more precise calculations of ion escape.

Through this analysis, we also found that ion escape on the nightside of Mars appears to be primarily limited by supply, and would therefore be enhanced effectively by any processes that increase nightside ion production (e.g., energetic electron precipitation). Ion escape on the dayside, however, appears to be limited by the energization and transport of ions. Because dayside ion escape higher than nightside ion escape by a factor of 10, this may suggest that the ion escape at Mars would be drastically increased by processes that increase energization and transport efficiency, particularly in unmagnetized regions on the Martian dayside.

Our results may hold implications toward the broader question of whether global magnetic dynamos are important for planetary habitability. In the context of planetary evolution, global magnetic fields are often described as critical for the retention of a planet's atmosphere, but it is currently unclear whether this is the case (Brain et al., 2013; Dandouras et al., 2020; Egan et al., 2019; Moore & Horwitz, 2007; Strangeway et al., 2010). We may be able to treat crustal fields as a microcosm through which we can characterize the effects of global-scale fields, and investigations of the kind presented here represent a significant step toward that goal. The extent to which crustal fields can truly be used to understand the influence of global dynamos is currently unclear, however, and is left to future studies.

Data Availability Statement

All MAVEN data used in this study are available through the Planetary Data System (https://pds-ppi.igpp.ucla.edu/mission/MAVEN). The data sets we used come from STATIC d1 measurements (https://pds-ppi.igpp.ucla.edu/data/maven-static-c/data/d1_g32e4d16a8m/), SWEA measurements (https://pds-ppi.igpp.ucla.edu/data/maven-swea-calibrated/data/), and MAG measurements (https://pds-ppi.igpp.ucla.edu/data/maven-mag-calibrated/data/).

References

Acuna, M., Connerney, J., Lin, R., Mitchell, D., Carlson, C., McFadden, J., et al. (1999). Global distribution of crustal magnetization discovered by the Mars global surveyor MAG/ER experiment. *Science*, *284*(5415), 790–793. https://doi.org/10.1126/science.284.5415.790

Andrews, D., Edberg, N. J., Eriksson, A. I., Gurnett, D., Morgan, D., Němec, F., & Opgenoorth, H. J. (2015). Control of the topside Martian ionosphere by crustal magnetic fields. *Journal of Geophysical Research: Space Physics*, *120*(4), 3042–3058. https://doi.org/10.1002/2014ja020703

Brain, D. A. (2007). Mars global surveyor measurements of the Martian solar wind interaction. In *The mars plasma environment* (pp. 77–112). Springer. https://doi.org/10.1007/978-0-387-70943-7_5

Brain, D. A., Bagenal, F., Acuña, M., & Connerney, J. (2003). Martian magnetic morphology: Contributions from the solar wind and crust. *Journal of Geophysical Research*, *108*(A12), 1424. https://doi.org/10.1029/2002ja009482

Brain, D. A., Leblanc, F., Luhmann, J., Moore, T. E., & Tian, F. (2013). *Planetary magnetic fields and climate evolution. CCTP* (p. 487).

Brain, D. A., McFadden, J., Halekas, J. S., Connerney, J., Bougher, S. W., Curry, S., et al. (2015). The spatial distribution of planetary ion fluxes near mars observed by MAVEN. *Geophysical Research Letters*, *42*(21), 9142–9148. https://doi.org/10.1002/2015gl065293

Brain, D. A., Weber, T., Xu, S., Mitchell, D., Lillis, R., Halekas, J., & Jakosky, B. (2020). Variations in nightside magnetic field topology at Mars. *Geophysical Research Letters*, *47*(19), e2020GL088921. https://doi.org/10.1029/2020gl088921

Brecht, S. H., & Ledvina, S. A. (2014). The role of the Martian crustal magnetic fields in controlling ionospheric loss. *Geophysical Research Letters*, *41*(15), 5340–5346. https://doi.org/10.1002/2014gl060841

Büchner, J., & Zelenyi, L. M. (1989). Regular and chaotic charged particle motion in magnetotaillike field reversals: 1. Basic theory of trapped motion. *Journal of Geophysical Research*, *94*(A9), 11821–11842. https://doi.org/10.1029/ja094ia09p11821

Collinson, G., Glocer, A., Xu, S., Mitchell, D., Frahm, R. A., Grebowsky, J., et al. (2019). Ionospheric ambipolar electric fields of Mars and Venus: Comparisons between theoretical predictions and direct observations of the electric potential drop. *Geophysical Research Letters*, *46*(3), 1168–1176. https://doi.org/10.1029/2018gl080597

Connerney, J., Espley, J., Lawton, P., Murphy, S., Odom, J., Oliversen, R., & Sheppard, D. (2015). The MAVEN magnetic field investigation. *Space Science Reviews*, *195*(1–4), 257–291. https://doi.org/10.1007/s11214-015-0169-4

Crider, D. H., Acuña, M. H., Connerney, J. E., Vignes, D., Ness, N. F., Krymskii, A. M., et al. (2002). Observations of the latitude dependence of the location of the Martian magnetic pileup boundary. *Geophysical Research Letters*, *29*(8), 11-1–11-4. https://doi.org/10.1029/2001gl013860

Dandouras, I., Blanc, M., Fossati, L., Gerasimov, M., Guenther, E. W., Kislyakova, K. G., et al. (2020). Future missions related to the determination of the elemental and isotopic composition of earth, moon and the terrestrial planets. *Space Science Reviews*, *216*(8), 1–49. https://doi.org/10.1007/s11214-020-00736-0

DiBraccio, G. A., Luhmann, J. G., Curry, S. M., Espley, J. R., Xu, S., Mitchell, D. L., & Harada, Y. (2018). The twisted configuration of the Martian magnetotail: MAVEN observations. *Geophysical Research Letters*, *45*, 4559–4568. https://doi.org/10.1029/2018gl077251

Dong, Y., Fang, X., Brain, D., McFadden, J., Halekas, J., Connerney, J., et al. (2015). Strong plume fluxes at Mars observed by MAVEN: An important planetary ion escape channel. *Geophysical Research Letters*, *42*(21), 8942–8950. https://doi.org/10.1002/2015gl065346

Dong, Y., Fang, X., Brain, D., McFadden, J., Halekas, J., Connerney, J., et al. (2017). Seasonal variability of Martian ion escape through the plume and tail from MAVEN observations. *Journal of Geophysical Research: Space Physics*, *122*(4), 4009–4022. https://doi.org/10.1002/2016ja023517

Dubinin, E., Chanteur, G., Fraenz, M., & Woch, J. (2008). Field-aligned currents and parallel electric field potential drops at Mars. Scaling from the Earth' aurora. *Planetary and Space Science*, *56*(6), 868–872. https://doi.org/10.1016/j.pss.2007.01.019

Dubinin, E., Fränz, M., Pätzold, M., Woch, J., McFadden, J., Fan, K., & Zelenyi, L. (2020). Impact of Martian crustal magnetic field on the ion escape. *Journal of Geophysical Research: Space Physics*, *125*(10), e2020JA028010. https://doi.org/10.1029/2020ja028010

Edberg, N., Lester, M., Cowley, S., & Eriksson, A. (2008). Statistical analysis of the location of the Martian magnetic pileup boundary and bow shock and the influence of crustal magnetic fields. *Journal of Geophysical Research*, *113*(A8), A08206. https://doi.org/10.1029/2008ja013096

Edberg, N., Nilsson, H., Williams, A., Lester, M., Milan, S., Cowley, S., & Futaana, Y. (2010). Pumping out the atmosphere of mars through solar wind pressure pulses. *Geophysical Research Letters*, *37*(3), L03107. https://doi.org/10.1029/2009gl041814

Egan, H., Jarvinen, R., Ma, Y., & Brain, D. (2019). Planetary magnetic field control of ion escape from weakly magnetized planets. *Monthly Notices of the Royal Astronomical Society*, *488*(2), 2108–2120. https://doi.org/10.1093/mnras/stz1819

Ergun, R., Andersson, L., Fowler, C., Woodson, A., Weber, T., Delory, G., et al. (2016). Enhanced O^{2+} loss at mars due to an ambipolar electric field from electron heating. *Journal of Geophysical Research: Space Physics*, *121*, 4668–4678. https://doi.org/10.1002/2016JA022349

Ergun, R., Andersson, L., Peterson, W., Brain, D., Delory, G., Mitchell, D., & Yau, A. (2006). Role of plasma waves in Mars' atmospheric loss. *Geophysical Research Letters*, *33*(14), L14103. https://doi.org/10.1029/2006gl025785

Espley, J. R. (2018). The Martian magnetosphere: Areas of unsettled terminology. *Journal of Geophysical Research: Space Physics*, *123*(6), 4521–4525. https://doi.org/10.1029/2018ja025278

Fang, X., Liemohn, M. W., Nagy, A. F., Luhmann, J. G., & Ma, Y. (2010). On the effect of the Martian crustal magnetic field on atmospheric erosion. *Icarus*, *206*(1), 130–138. https://doi.org/10.1016/j.icarus.2009.01.012

Fang, X., Ma, Y., Brain, D., Dong, Y., & Lillis, R. (2015). Control of Mars global atmospheric loss by the continuous rotation of the crustal magnetic field: A time-dependent MHD study. *Journal of Geophysical Research: Space Physics*, *120*(12), 10–926. https://doi.org/10.1002/2015ja021605

Fang, X., Ma, Y., Masunaga, K., Dong, Y., Brain, D., Halekas, J., et al. (2017). The Mars crustal magnetic field control of plasma boundary locations and atmospheric loss: MHD prediction and comparison with MAVEN. *Journal of Geophysical Research: Space Physics*, *122*(4), 4117–4137. https://doi.org/10.1002/2016ja023509

Fowler, C., Andersson, L., Ergun, R., Morooka, M., Delory, G., Andrews, D. J., et al. (2015). The first in situ electron temperature and density measurements of the Martian nightside ionosphere. *Geophysical Research Letters*, *42*(21), 8854–8861. https://doi.org/10.1002/2015gl065267

Fowler, C. M., Agapitov, O. V., Xu, S., Mitchell, D. L., Andersson, L., Artemyev, A. et al. (2020). Localized heating of the Martian topside ionosphere through the combined effects of magnetic pumping by large-scale magnetosonic waves and pitch angle diffusion by whistler waves. *Geophysical Research Letters*, *47*(5), e2019GL086408. https://doi.org/10.1029/2019GL086408

Fox, J. L., Brannon, J., & Porter, H. (1993). Upper limits to the nightside ionosphere of Mars. *Geophysical Research Letters*, *20*(13), 1339–1342. https://doi.org/10.1029/93gl01349

Frahm, R., Sharber, J., Winningham, J., Wurz, P., Liemohn, M., Kallio, E., et al. (2006). Locations of atmospheric photoelectron energy peaks within the Mars environment. *Space Science Reviews*, *126*(1–4), 389–402.

Jakosky, B. M., Brain, D., Chaffin, M., Curry, S., Deighan, J., Grebowsky, J., et al. (2018). Loss of the Martian atmosphere to space: Present-day loss rates determined from MAVEN observations and integrated loss through time. *Icarus*, *315*, 146–157. https://doi.org/10.1016/j.icarus.2018.05.030

Jakosky, B. M., Grebowsky, J. M., Luhmann, J. G., Connerney, J., Eparvier, F., Ergun, R., et al. (2015a). MAVEN observations of the response of Mars to an interplanetary coronal mass ejection. *Science*, *350*(6261), aad0210. https://doi.org/10.1126/science.aad0210

Jakosky, B. M., Lin, R., Grebowsky, J., Luhmann, J., Mitchell, D., Beutelschies, G., et al. (2015b). The Mars atmosphere and volatile evolution (MAVEN) mission. *Space Science Reviews*, *195*(1–4), 3–48. https://doi.org/10.1007/s11214-015-0139-x

Liemohn, M. W., Ma, Y., Frahm, R. A., Fang, X., Kozyra, J. U., Nagy, A. F., et al. (2007). Mars global MHD predictions of magnetic connectivity between the dayside ionosphere and the magnetospheric flanks. In *The Mars plasma environment* (pp. 63–76). Springer. https://doi.org/10.1007/978-0-387-70943-7_4

Lundin, R., & Hultqvist, B. (1989). Ionospheric plasma escape by high-altitude electric fields: Magnetic moment "pumping". *Journal of Geophysical Research*, *94*(A6), 6665–6680. https://doi.org/10.1029/ja094ia06p06665

Lundin, R., Barabash, S., Holmström, M., Nilsson, H., Yamauchi, M., Fraenz, M., & Dubinin, E. (2008). A comet-like escape of ionospheric plasma from Mars. *Geophysical Research Letters*, *35*(18), L18203. https://doi.org/10.1029/2008gl034811

Lundin, R., Barabash, S., Yamauchi, M., Nilsson, H., & Brain, D. (2011). On the relation between plasma escape and the Martian crustal magnetic field. *Geophysical Research Letters*, *38*(2), L02102. https://doi.org/10.1029/2010gl046019

Lundin, R., Winningham, D., Barabash, S., Frahm, R., Holmström, M., Sauvaud, J.-A., et al. (2006). Plasma acceleration above Martian magnetic anomalies. *Science*, *311*(5763), 980–983. https://doi.org/10.1126/science.1122071

Lundin, R., Zakharov, A., Pellinen, R., Barabasj, S., Borg, H., Dubinin, E., et al. (1990). ASPERA/PHOBOS measurements of the ion outflow from the Martian ionosphere. *Geophysical Research Letters*, *17*(6), 873–876. https://doi.org/10.1029/gl017i006p00873

Matsunaga, K., Seki, K., Brain, D. A., Hara, T., Masunaga, K., Mcfadden, J. P., et al. (2017). Statistical study of relations between the induced magnetosphere, ion composition, and pressure balance boundaries around mars based on MAVEN observations. *Journal of Geophysical Research: Space Physics*, *122*(9), 9723–9737. https://doi.org/10.1002/2017ja024217

Ma, Y., Fang, X., Russell, C. T., Nagy, A. F., Toth, G., Luhmann, J. G., et al. (2014). Effects of crustal field rotation on the solar wind plasma interaction with Mars. *Geophysical Research Letters*, *41*(19), 6563–6569. https://doi.org/10.1002/2014gl060785

McFadden, J., Kortmann, O., Curtis, D., Dalton, G., Johnson, G., Abiad, R., et al. (2015). MAVEN suprathermal and thermal ion composition (static) instrument. *Space Science Reviews*, *195*(1–4), 199–256. https://doi.org/10.1007/s11214-015-0175-6

Mitchell, D., Lin, R., Mazelle, C., Rème, H., Cloutier, P., Connerney, J., et al. (2001). Probing Mars' crustal magnetic field and ionosphere with the MGS electron reflectometer. *Journal of Geophysical Research: Planets*, *106*(E10), 23419–23427. https://doi.org/10.1029/2000je001435

Mitchell, D., Mazelle, C., Sauvaud, J.-A., Thocaven, J.-J., Rouzaud, J., Fedorov, A., et al. (2016). The MAVEN solar wind electron analyzer. *Space Science Reviews*, *200*(1–4), 495–528. https://doi.org/10.1007/s11214-015-0232-1

Moore, T. E., & Horwitz, J. (2007). Stellar ablation of planetary atmospheres. *Reviews of Geophysics*, *45*(3), RG3002. https://doi.org/10.1029/2005rg000194

Morschhauser, A., Lesur, V., & Grott, M. (2014). A spherical harmonic model of the lithospheric magnetic field of Mars. *Journal of Geophysical Research: Planets*, *119*(6), 1162–1188. https://doi.org/10.1002/2013je004555

Nilsson, H., Carlsson, E., Brain, D. A., Yamauchi, M., Holmström, M., Barabash, S., et al. (2010). Ion escape from Mars as a function of solar wind conditions: A statistical study. *Icarus*, *206*(1), 40–49. https://doi.org/10.1016/j.icarus.2009.03.006

Nilsson, H., Edberg, N. J., Stenberg, G., Barabash, S., Holmström, M., Futaana, Y., et al. (2011). Heavy ion escape from Mars, influence from solar wind conditions and crustal magnetic fields. *Icarus*, *215*(2), 475–484. https://doi.org/10.1016/j.icarus.2011.08.003

Ramstad, R., Barabash, S., Futaana, Y., & Holmström, M. (2017). Solar wind-and EUV-dependent models for the shapes of the Martian plasma boundaries based on mars express measurements. *Journal of Geophysical Research: Space Physics*, *122*(7), 7279–7290. https://doi.org/10.1002/2017ja024098

Ramstad, R., Barabash, S., Futaana, Y., Nilsson, H., & Holmström, M. (2016). Effects of the crustal magnetic fields on the Martian atmospheric ion escape rate. *Geophysical Research Letters*, *43*(20), 10–574. https://doi.org/10.1002/2016gl070135

Ramstad, R., Barabash, S., Futaana, Y., Nilsson, H., & Holmström, M. (2017). Global Mars-solar wind coupling and ion escape. *Journal of Geophysical Research: Space Physics*, *122*(8), 8051–8062. https://doi.org/10.1002/2017ja024306

Ramstad, R., Barabash, S., Futaana, Y., Nilsson, H., Wang, X.-D., & Holmström, M. (2015). The Martian atmospheric ion escape rate dependence on solar wind and solar EUV conditions: 1. Seven years of Mars express observations. *Journal of Geophysical Research: Planets*, *120*(7), 1298–1309. https://doi.org/10.1002/2015je004816

Ribas, I., Guinan, E. F., Güdel, M., & Audard, M. (2005). Evolution of the solar activity over time and effects on planetary atmospheres. I. High-energy irradiances (1-1700 å). *The Astrophysical Journal*, *622*(1), 680–694. https://doi.org/10.1086/427977

Steckiewicz, M., Garnier, P., André, N., Mitchell, D., Andersson, L., Penou, E., et al. (2017). Comparative study of the Martian suprathermal electron depletions based on Mars global surveyor, Mars express, and Mars atmosphere and volatile evolution mission observations. *Journal of Geophysical Research: Space Physics*, *122*(1), 857–873. https://doi.org/10.1002/2016ja023205

Strangeway, R., Russell, C., Luhmann, J., Moore, T., Foster, J., Barabash, S., & Nilsson, H. (2010). Does a planetary-scale magnetic field enhance or inhibit ionospheric plasma outflows? AGUFM, 2010. SM33B-1893.

Vaisberg, O., Smirnov, V., & Omelchenko, A. (1977). Solar wind interaction with Martian magnetosphere. STIN, 78, 23000.

Weber, T., Brain, D., Mitchell, D., Xu, S., Connerney, J., & Halekas, J. (2017). Characterization of low-altitude nightside Martian magnetic topology using electron pitch angle distributions. *Journal of Geophysical Research: Space Physics*, *122*(10), 9777–9789. https://doi.org/10.1002/2017ja024491

Weber, T., Brain, D., Mitchell, D., Xu, S., Espley, J., Halekas, J., & Jakosky, B. (2019). The influence of solar wind pressure on Martian crustal magnetic field topology. *Geophysical Research Letters*, *46*, 2347–2354. https://doi.org/10.1029/2019gl081913

Weber, T., Brain, D., Mitchell, D., Xu, S., Espley, J., Halekas, J., & Jakosky, B. (2020). The influence of interplanetary magnetic field direction on the topology of Martian crustal field cusps. *Geophysical Research Letters*, *47*, e2020GL087757. https://doi.org/10.1029/2020GL087757

Wood, B. E. (2006). The solar wind and the sun in the past. *Space Science Reviews*, *126*(1–4), 3–14. https://doi.org/10.1007/s11214-006-9006-0

Xu, S., Mitchell, D. L., Liemohn, M., Fang, X., Ma, Y., Luhmann, J., et al. (2017). Martian low-altitude magnetic topology deduced from MAVEN/SWEA observations. *Journal of Geophysical Research: Space Physics*, *122*(2), 1831–1852. https://doi.org/10.1002/2016JA023467

Xu, S., Mitchell, D. L., McFadden, J. P., Collinson, G., Harada, Y., Lillis, R., & Connerney, J. (2018). Field-aligned potentials at Mars from MAVEN observations. *Geophysical Research Letters*, *45*(19), 10–119. https://doi.org/10.1029/2018gl080136

Xu, S., Mitchell, D. L., McFadden, J. P., Fillingim, M. O., Andersson, L., Brain, D. A., et al. (2020a). Inverted-v electron acceleration events concurring with localized auroral observations at Mars by MAVEN. *Geophysical Research Letters*, *47*(9), e2020GL087414. https://doi.org/10.1029/2020gl087414

Xu, S., Mitchell, D. L., Weber, T., Brain, D. A., Luhmann, J. G., Dong, C., et al. (2020b). Characterizing Mars's magnetotail topology with respect to the upstream interplanetary magnetic fields. *Journal of Geophysical Research: Space Physics*, *125*(3), e2019JA027755. https://doi.org/10.1029/2019ja027755

Xu, S., Weber, T., Mitchell, D. L., Brain, D. A., Mazelle, C., DiBraccio, G. A., & Espley, J. (2019). A technique to infer magnetic topology at Mars and its application to the terminator region. *Journal of Geophysical Research: Space Physics*, *124*, 1823–1842. https://doi.org/10.1029/2018ja026366

Zhang, Y., Shen, C., Marchaudon, A., Rong, Z., Lavraud, B., Fazakerley, A., et al. (2016). First in situ evidence of electron pitch angle scattering due to magnetic field line curvature in the ion diffusion region. *Journal of Geophysical Research: Space Physics*, *121*(5), 4103–4110. https://doi.org/10.1002/2016ja022409